University of Central Lancashire
UCLan

Central Lancashire Online Knowledge (CLoK)

Title	Metal–Organic Framework MIL-101(Fe) Nanoparticles Decorated with Ag Nanoparticles for Regulating the Photocatalytic Phenol Oxidation Pathway for Cr(VI) Reduction
Type	Article
URL	https://clok.uclan.ac.uk/37582/
DOI	https://doi.org/10.1021/acsanm.1c00119
Date	2021
Citation	Gong, Jianqiu, Zhang, Weiwei, Sen, Tapas, Yu, Yichen, Liu, Yuchen, Zhang, Jinlong and Wang, Lingzhi (2021) Metal–Organic Framework MIL-101(Fe) Nanoparticles Decorated with Ag Nanoparticles for Regulating the Photocatalytic Phenol Oxidation Pathway for Cr(VI) Reduction. ACS Applied Nano Materials, 4 (5). pp. 4513-4521.
Creators	Gong, Jianqiu, Zhang, Weiwei, Sen, Tapas, Yu, Yichen, Liu, Yuchen, Zhang, Jinlong and Wang, Lingzhi

It is advisable to refer to the publisher's version if you intend to cite from the work.
https://doi.org/10.1021/acsanm.1c00119

For information about Research at UCLan please go to http://www.uclan.ac.uk/research/

All outputs in CLoK are protected by Intellectual Property Rights law, including Copyright law. Copyright, IPR and Moral Rights for the works on this site are retained by the individual authors and/or other copyright owners. Terms and conditions for use of this material are defined in the http://clok.uclan.ac.uk/policies/

Metal-Organic Framework MIL-101(Fe) Nanoparticles Decorated with Ag Nanoparticles for Regulating the Photocatalytic Phenol Oxidation Pathway for Cr(VI) Reduction

Jianqiu Gong[†], Weiwei Zhang[†], Tapas Sen[‡], Yichen Yu, Yuchen Liu, Jinlong Zhang[†], Lingzhi Wang[†,]*

[†] Shanghai Engineering Research Center for Multi-media Environmental Catalysis and Resource Utilization, Key Lab for Advanced

Materials and Joint International Research Laboratory of Precision Chemistry and Molecular Engineering, Feringa Nobel Prize Scientist Joint Research Center, Institute of Fine Chemicals, School of Chemistry and Molecular Engineering, East China University of Science & Technology, 130 Meilong Road, Shanghai, 200237, China.

[‡]School of Physical Sciences & Computing, Centre of Materials Sciences, University Of Central Lancashire, Preston, UK.

ABSTRACT

Photocatalysis is a promising technology to treat dilute phenol-Cr(VI) mixture, where photo-induced electrons are commonly thought of as the main active species for Cr(VI) reduction. However, it generally depends on the surface adsorption to achieve efficient electron transfer. Meanwhile, the possible contribution of reductive quinone derivatives oxidized from phenol to Cr(VI) reduction has been rarely explored. The key is to explicitly understand the relation between the phenol oxidation pathway and Cr(VI) reduction. Herein, Ag/AgCl/MIL-101(Fe) prepared by directly loading Ag nanoparticles on MIL-101(Fe) was applied to the joint treatment of phenol and Cr(VI). The role of quinone derivatives in reducing Cr(VI) was revealed by excluding the surface adsorption. During the phenol oxidation, ·OH radicals were more consumed in the initial stage for the ring-opening of phenol. Meanwhile, $^1O_2$ evolved from $\cdot O_2^-$ gradually caused the accumulation of reductive quinone intermediates, which dramatically accelerated the Cr(VI) reduction afterwards. This study demonstrates the significance of controlling the evolution process of active oxygen species for the joint photocatalytic treatment of phenol-Cr(VI) mixture.

Keywords: Photocatalysis; Ag/AgCl/MIL-101(Fe); Cr(VI) reduction; phenol degradation; quinone derivatives; $^1O_2$

1. INTRODUCTION

Phenol and Cr(VI) are the commonly coexistent pollutants discharged from the leather tanning and wood products industries.[1-5] Reactions between them can reduce Cr(VI) to less toxic Cr(III) but generally occurs under strongly acid conditions with high concentrations.[6, 7] Photocatalysis has been commonly used to reduce Cr(VI) and degrade phenol with comparatively lower concentrations;[8-12] photo-induced electrons are thought as the main active species for Cr(VI) reduction.[13-16] Therefore, photocatalysts with high activity generally have enhanced hole-electron separation efficiency.[17-22] This case is not vice versa since the electron-induced Cr(VI) reduction requires efficient surface adsorption of anion Cr(VI) on the photocatalyst, which restricts the photocatalysts with low isoelectric points to strongly acid conditions.[23-26]

Meanwhile, the quinone derivatives oxidized from phenol, including hydroquinone (HQ) and semiquinone (SQ), are effective for Cr(VI) reduction. It is highly possible that these intermediates could also contribute to the Cr(VI) reduction during photocatalysis, which is however, hard to determine since the concentration may be dynamically varied with the reaction phase. For example, quinone derivatives can be formed in the presence of different active oxygen species including ·OH,[27, 28] $\cdot O_2^-$,[29, 30] and $^1O_2$,[31-33] but may undergo fast ring-opening reaction when further attacked by aggressive ·OH radicals.[34-37] On the other hand, the active oxygen species of ·OH, $\cdot O_2^-$ and $^1O_2$ in the photocatalytic system can mutually transform to each other under certain conditions,[38, 39] which further complicates the situation about exploring the reduction effect of quinone derivatives. An explicit understanding of the role of quinone derivatives in reducing Cr(VI) is necessary to help us extrapolate to the complex systems of waste phenol-Cr(VI) mixtures, which requires the fine unraveling of the formation-evolution of active oxygen species.

MOFs with high specific surface area and highly tunable structure characteristics have shown promising potential in photocatalytic water decontamination.[40-44] The abundant structure characteristics of MOFs provide diversified options for the tuning of interfacial interaction.[45-48] Herein, Ag/AgCl/MIL-101(Fe) was fabricated by simply

loading Ag nanoparticles on MIL-101(Fe) and applied to the photocatalytic treatment of phenol-Cr(VI). It showed a cooperation effect for the phenol degradation and Cr(VI) reduction with excellent cyclic stability under weak acid to near-neutral conditions. The evolution of active oxygen species including ·OH and $^1O_2$ under visible light irradiation and their relation with the phenol oxidation and Cr(VI) reduction were explicitly explored. The former caused the fast ring-opening of phenol in the initial phase, and the latter caused the gradual accumulation of quinone derivatives. The contribution of quinone derivatives to Cr(VI) reduction was identified besides the photo-induced electrons. This study provides a new way for photocatalytic Cr(VI) reduction in mixed phenol-Cr(VI) system by regulating the photocatalytic oxidation pathway of phenol.

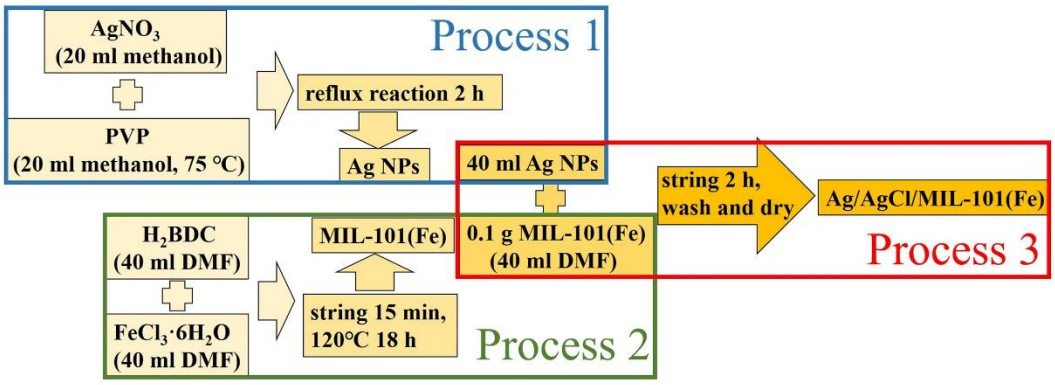

Scheme 1. Synthesis of Ag/AgCl/MIL-101.

2. EXPERIMENTAL SECTION

2.1. Chemicals and Materials. N, N-dimethyl formamide (DMF, 99.8wt%), 1,4-benzenedicarboxylate (H_2BDC, 99wt%), silver nitrate ($AgNO_3$, 99.8wt%) and methanol were purchased from Aladdin industrial corporation (Shanghai, China). Anhydrous ethanol, potassium dichromate, iron(III) chloride hexahydrate ($FeCl_3·6H_2O$, 99wt%) and polyvinylpyrrolidone (PVP, K-30) were purchased from Sinopharm Chemical Reagent Co., Ltd., China. All the chemicals were used without further purification.

2.2. Synthesis of Ag nanoparticles. In the synthesis process of Ag nanoparticles (NPs),

85 mg $AgNO_3$ and 60 mg PVP were used to prepare Ag NPs for 0.5% Ag/AgCl/MIL-101(Fe), 170 mg $AgNO_3$ and 120 mg PVP were used to prepare Ag NPs for 1% Ag/AgCl/MIL-101(Fe), and 340 mg $AgNO_3$ and 180 mg PVP were used to prepare Ag NPs for 2% Ag/AgCl/MIL-101(Fe). In a typical procedure, $AgNO_3$ and PVP were added to two beakers with 20 mL methanol, respectively. The $AgNO_3$ solution was then added into the PVP solution drop by drop. Finally, the mixture was heated to 75 °C under magnetic stirring and maintained for 2 h (Scheme 1, Process 1). When the reaction was complete, the solution was cooled to room temperature and used for the next step.

2.3. Synthesis of MIL-101(Fe). The MIL-101(Fe) was fabricated using a simple solvothermal method reported previously.[49] In a typical procedure, 0.766 g H_2BDC and 1.246 g $FeCl_3 \cdot 6H_2O$ were added to 40 ml DMF respectively. After stirring 15 min, the mixture was transferred to a Teflon-lined stainless steel autoclave and placed in an oven at 120 ℃ for 18 h (Scheme 1, Process 2). The obtained products were washed with DMF, deionized water and ethanol, and dried prior to use.

2.4. Synthesis of Ag/AgCl/MIL-101(Fe). 40 mL as-synthesized Ag NPs solution was added drop by drop into 40 mL DMF of MIL-101(Fe) (0.1 g) under vigorous stirring, and then the mixed solution was further stirred at room temperature for 2 h. Subsequently, the sample was centrifuged at 10000 rpm for 5 minutes, washed with numerous ethanol and ultrapure water, and dried at 60 ^oC in a vacuum oven (Scheme 1, Process 3). The dark yellow solid powder obtained is Ag/AgCl/MIL-101(Fe). Ag/AgCl was prepared from $FeCl_3$ and Ag NPs, and used as the control sample.

2.5. Photocatalytic Tests. The Cr(VI) reduction and the phenol degradation were tested under visible-light irradiation by using a xenon lamp equipped with a light filter (≥420 nm, 300 W). In a typical experiment, 50 mg Ag/AgCl/MIL-101(Fe) was suspended in 50 mL of 10 mg/L Cr(VI) and phenol solution. The pH was tuned to 6 to prevent the formation of precipitation. [50] The mixture was stirred for 30 min without light to reach

the adsorption-desorption equilibrium. During visible-light irradiation, a certain amount of liquid was taken out to analyze every 15 minutes. The concentration of Cr(VI) was determined by the diphenylcarbazide (DPC) method. The concentration of phenol was measured by a high-performance liquid chromatography (HPLC) system.

2.6 Characterization. Transmission electron microscopy (TEM) was conducted on a JEOL JEM-2100EX electron microscope, operated at an accelerating voltage of 200 kV. X-ray diffraction (XRD) measurements were performed with a Rigaku Ultima IV (Cu Ka radiation, λ=1.5406 Å) in the range of 5-80° (2θ). The instrument employed for X-ray photoelectron spectrum (XPS) measurements was a PerkinElmer PHI 5000C ESCA system with Al Kα radiation operated at 250 W. The UV-vis absorption spectroscopy was measured with a Shimadzu UV-2450 spectrometer. Phenol values were monitored using a SHIMADZU SPD-M20A reverse-phase high-performance liquid chromatography (HPLC) system at a flow rate of 1 $mL \cdot min^{-1}$ with a RX-C18 column (4.6 × 250 mm, 5 μm). The detection of radicals was carried out on a 100G-18KG/EMX-8/2.7 Electro-Spin Resonance spectrometer.

3. RESULTS AND DISCUSSION

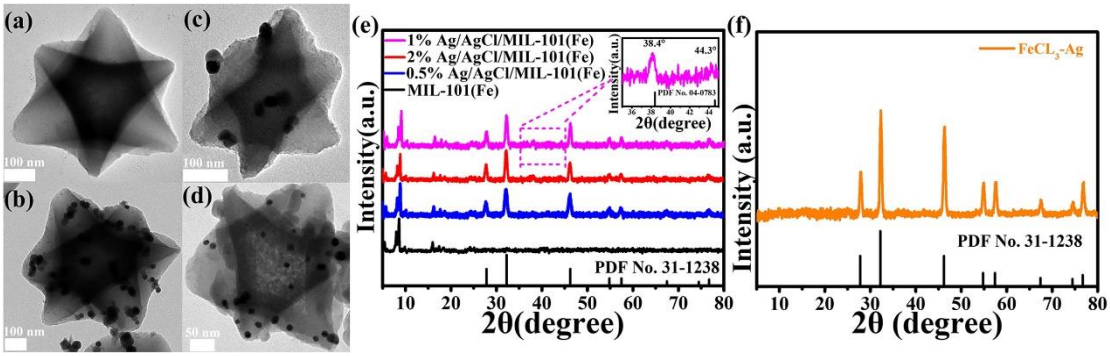

Figure 1. (a-d) TEM images of MIL-101(Fe), 0.5% Ag/AgCl/MIL-101(Fe), 1% Ag/AgCl/MIL-101(Fe) and 2% Ag/AgCl/MIL-101(Fe); (e) XRD patterns of different samples; (f) XRD pattern of Ag/AgCl.

3.1. Structure Characterization. Ag/AgCl/MIL-101(Fe) heterojunction was fabricated via the reaction between Ag NPs and the Fe(III)-Cl in the framework of MIL-101(Fe). As shown in Figure 1a, the TEM images of MIL-101(Fe) show an approximately hexagonal shape with an edge length of ca. 550 nm. After the loading of

Ag nanoparticles, the hexagonal shape becomes less ordered with coarsened and blurred edges, indicating the possible reaction between Ag and MIL-101(Fe) (Figure 1b-d, S1). The NPs have an average size of ca. 20 nm and become more agglomerate at higher loading content. According to the high-resolution TEM (HRTEM) image of sample 1% Ag/AgCl/MIL-101(Fe), the loaded NPs have lattice fringes of d=0.201 nm and d=0.277 nm (Figure S2), corresponding to the Ag (2 0 0) and AgCl (2 0 0) planes, respectively. These results demonstrate the formation of Ag/AgCl composites on MIL-101(Fe).

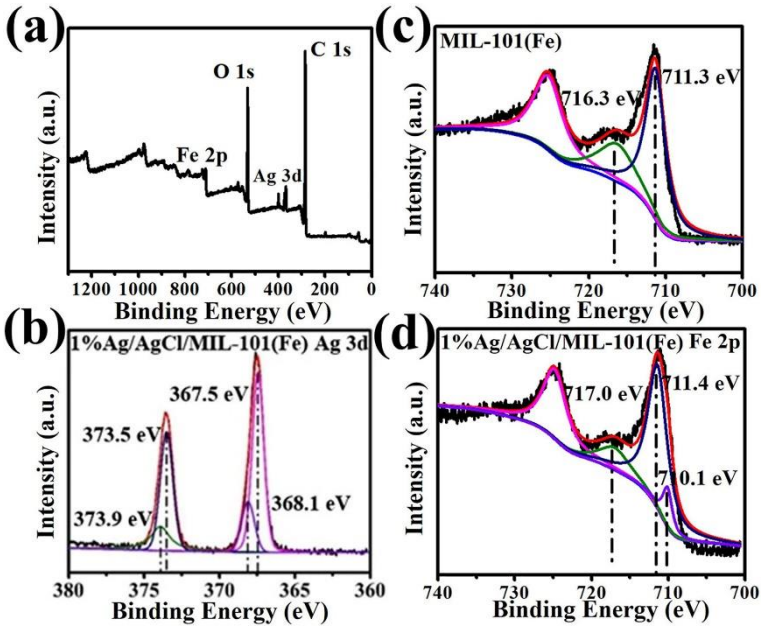

Figure 2. (a) XPS survey spectrum of 1% Ag/AgCl/MIL-101(Fe); (b) Ag3d spectra of 1% Ag/AgCl/MIL-101(Fe); Fe2p spectra of (c) MIL-101 and (d) 1% Ag/AgCl/MIL-101.

The XRD measurement was performed to characterize the crystal structures of samples loaded with different amounts of Ag. The obvious peaks at 27.7 °, 32.4 °, 46.3 °, 54.9 ° and 57.7 ° correspond to the (1 1 1), (2 0 0), (2 2 0), (3 1 1) and (2 2 2) planes of AgCl (Figure 1f, JCPDS No. 31-1238). The amplified signal at 38.4 ° is assigned to the (1 1 1) crystal plane of Ag (JCPDS No. 04-0783). No other obvious characteristic peaks of Ag NPs can be observed (Figure 1e, f), which may be attributed to the small size or small amounts of Ag, suggesting most of Ag should be oxidized to AgCl. The above results further confirm that the Ag/AgCl/MIL-101(Fe) ternary composite should be formed by simply loading Ag on MIL-101(Fe). The loading of Ag/AgCl is further

verified by the significantly decreased specific surface area and pore size of MIL-101 (Figure S3). The XPS survey spectrum confirms Ag, Fe and Cl species in the composite (Figure 2a). The small peaks at 367.5 and 373.9 eV are attributed to metallic Ag (Figure 2b). The MIL-101(Fe) only shows the peaks of Fe (III) at 711.3 eV (Figure 2c). After the loading of Ag, the signal of Fe (II) (Figure 2d) appears as characterized by the peak at 710.1 eV (ca. 9.0%), which should be attributed to the reaction shown in Eq. 1.

$$\text{MIL-101(Fe(III))} + \text{Ag}^0 \longrightarrow \text{Ag/AgCl/MIL-101(Fe(II, III))} \qquad (1)$$

The UV-Vis absorption spectra of MIL-101(Fe) and Ag/AgCl/MIL-101(Fe) composites are shown in Figure S4. The absorption band around 230 nm is attributed to the charge transfer from O to Fe in the octahedral coordination environment.[51] The absorption from 320 nm to the visible region is derived from the charge transfer from the ligand to the Fe-O cluster (LMCT).[52] AgCl has a strong light absorption in the UV region and the absorption in the visible region is attributed to the surface plasmon resonance (SPR) effect of noble Ag.

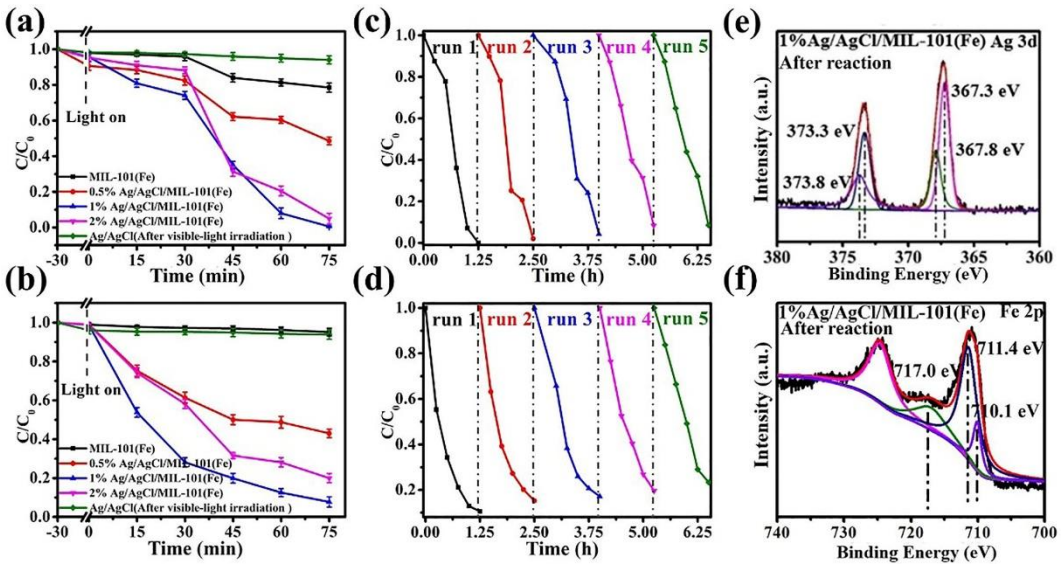

Figure 3. (a) Cr(VI) reduction and (b) phenol degradation via different samples in the phenol-Cr(VI) mixture; cyclic test for (c) Cr(VI) reduction and (d) phenol degradation in the phenol-Cr(VI) mixture; (e) Ag3d and (f) Fe2p XPS spectra of 1% Ag/AgCl/MIL-101(Fe) after reaction.

3.2. Photocatalytic test. The photocatalytic test was carried out in a mixed solution containing 10 mg/L of Cr(VI) and 10 mg/L of phenol under the irradiation of a 300 W xenon lamp equipped with a 420 nm filter. The photocatalytic reduction efficiency of

Cr(VI) first increases with the increasing amount of Ag and reaches almost 100% on sample 1% Ag/AgCl/MIL-101(Fe) (Figure 3a, S5). It is noted that the Cr(VI) reduction is obviously accelerated after irradiation for 30 min. Meanwhile, either Ag/AgCl or MIL-101(Fe) with the amount equivalent to the counterparts in the Ag/AgCl/MIL-101(Fe) composite shows negligible activity for Cr(VI) reduction, implying the activity should be attributed to the cooperative effect between Ag/AgCl and MIL-101(Fe). For the phenol degradation, sample 1% Ag/AgCl/MIL-101(Fe) also shows the best activity (Figure 3b), where ca. 70% of phenol can be degraded within the first 30 min. From the linear portion of this plot, the apparent quantum efficiency of phenol is 0.31% (Supplementary Text S1). In comparison, the loading of other noble metals including Au and Pt results in less efficient phenol degradation and Cr(VI) reduction (Table S1). To understand the photocatalytic process, the Cr(VI) reduction and phenol degradation were also carried out in the single systems (Figure S6a). The Cr(VI) reduction is significantly retarded in the absence of phenol (Figure S6b). In comparison, the degradation efficiency of phenol is less decreased (Figure S6c). Specifically, compared with the single-pollutant system, the Cr(VI) reduction and phenol oxidation are increased by 82% and 24% in the mixed system, respectively. The above results demonstrate the cooperative effect between Cr(VI) reduction and phenol oxidation, and the Cr(VI) reduction is more efficiently promoted in the mixed system.

In order to evaluate the stability of the composites, cyclic experiments were performed over 1% Ag/AgCl/MIL-101(Fe). The activity can be well preserved after five cyclic experiments (Figure 3c, d). A slightly decreased activity should be due to the unavoidable sample loss during recycling. It is noted from the XPS spectrum that the peaks of metallic Ag increase after the reaction (Figure 3e), accompanied by the improved content of the Fe(II) (ca. 18.2%, Figure 3f), which, however, keeps almost unvaried from the second run (Figure S7). This result demonstrates the chemical valences of Fe and Ag species changed during the first run but soon reached equilibrium. However, the improved Ag content seems contradictory to the appearance of more Fe(II) since the formation of Ag is supposed to be attributed to the electrons transferred from

MIL-101(Fe), and the remained hole in MIL-101(Fe) is expected to form Fe(III). The specific reason for the valence variation in the first run will be discussed later. Meanwhile, negligible content variation is observed through the XPS survey spectra after the first-run reaction, which excludes the possibility and influence of the particle leaching (Figure S8). The leaching-resistance of the Ag from the composite should be attributed to the chemical anchoring of Ag/AgCl on MIL-101(Fe) through the Ag-Cl-Fe bond, which should also be beneficial to the interfacial carrier transfer. The highest and photocurrent and minimum impedance observed from 1% Ag/AgCl/MIL-101(Fe) verify the promoted charge transfer between different components through the Ag-Cl-Fe bond (Figure S9).

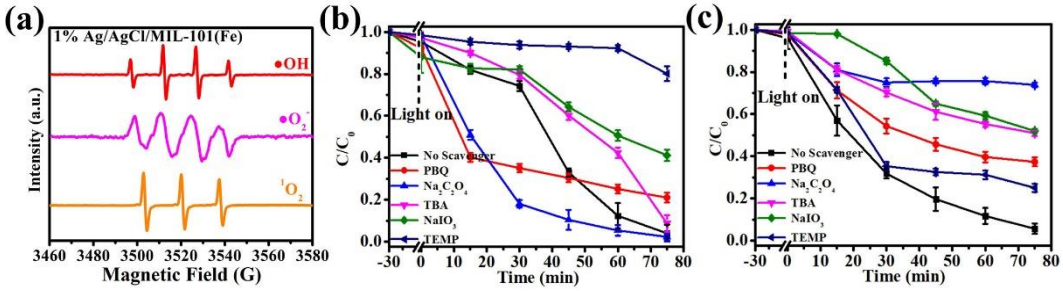

Figure 4. (a) EPR spectra for the detection of ·OH (water, DMPO); $\cdot O_2^-$ (methanol, DMPO); $^1O_2$ (water, 2, 2, 6, 6-tetramethylpiperidine (TEMP)); (b) phenol degradation and (c) Cr(VI) reduction with different radical scavengers in mixed systems.

3.3. Determination of active species. EPR was used to confirm the active species of phenol oxidation and Cr(VI) reduction (Figure 4a). Under visible-light irradiation, active oxygen species, including radicals ·OH and $\cdot O_2^-$, and non-radical $^1O_2$, can all be detected from the Ag/AgCl/MIL-101(Fe) composite. Photocatalytic experiments were carried out in the presence of different sacrificial agents to analyze the main active species responsible for Cr(VI) reduction and phenol degradation (Figure 4b, c). P-benzoquinone (PBQ), sodium oxalate ($Na_2C_2O_4$), tert-butanol (TBA), 2, 2, 6, 6-tetramethylpiperidine (TEMP), and sodium iodate ($NaIO_3$) were used to capture $\cdot O_2^-$, holes, ·OH, $^1O_2$ and electrons in the solution. For the phenol oxidation, the prohibition effect by hole capturer $Na_2C_2O_4$, ·OH capturer TBA, and $\cdot O_2^-$ capturer PBQ follows the order of $Na_2C_2O_4$ > TBA > PBQ (Figure 4b). Specifically, the former two show comparable prohibition effects and seem far more efficient than PBQ,

demonstrating OH evolved from holes should be the main active species for phenol degradation. Moreover, the significantly decreased activity for phenol in the presence of $NaIO_3$ should be ascribed to the oxidation of Ag by the hole that remained in the composite, demonstrating the essential role of the surface plasmon resonance (SPR) effect. A similar effect of the capturer agent on the phenol degradation was also observed in the single system (Figure S10). Based on the above results, OH radical should be the main active species for phenol degradation.

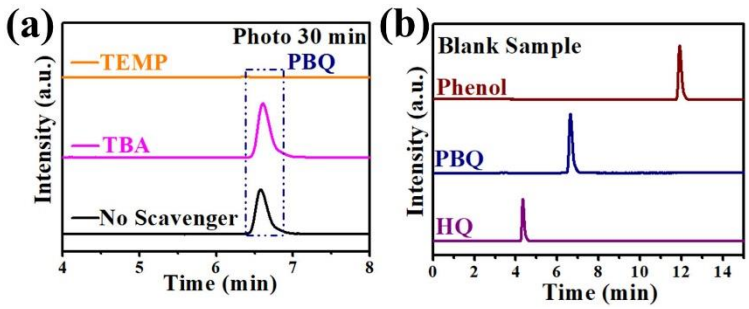

Figure 5. (a) HPLC chromatograms of reaction products of phenol degradation in the 1% Ag/Ag/MIL-101(Fe)/Cr(VI)/phenol/light system at 30 min. (PBQ (1 mM), TBA (2 mM), TEMP (5 mM)), (a) reserve time 0-8min, (b) blank phenol, PBQ and HQ.

For the Cr(VI) reduction (Figure 4c), TEMP most efficiently retards the Cr(VI) reduction, suggesting $^1O_2$ is the key species to induce the reduction. The contribution of Fe(II) to the Cr(VI) reduction should be excluded since more Fe(II) is formed during the first run, and the content keeps stable afterwards. It was reported HQ could be oxidized from phenol by $^1O_2$ (Eq. 2).[31, 34, 53] It is highly possible that HQ may cause the significantly promoted Cr(VI) reduction, which is consistent with the lagged Cr(VI) reduction compared with the phenol degradation. This consumption was supported by the enhanced Cr(VI) reduction in the presence of HQ under dark conditions (Figure S11). Moreover, according to the previous report, the reaction between HQ and Cr(VI) can successively produce SQ and PBQ (Eq. 3, 4).[54] The HPLC analysis of the product after 30 min irradiation in the presence of TEMP indicates the disappearance of PBQ signal (Figure 5), which further verifies the above consumption that $^1O_2$-induced HQ is responsible for the Cr(VI) reduction. The addition of PBQ to the photocatalysis system helps accelerate the Cr(VI) reduction within the first 15 minutes but decreases the

overall efficiency. It is assumed that PBQ consumes $\cdot O_2^-$ and produce SQ, which is also active for the Cr(VI) reduction (Eq. 4, 5); the gradually retarded Cr(VI) reduction suggests $^1O_2$ should be transformed from $\cdot O_2^-$ since the consumption of $\cdot O_2^-$ by PBQ is unfavorable to the formation of $^1O_2$. The decreased reduction rate of Cr(VI) in the presence of electron-capturer $NaIO_3$ should be related to the less efficient formation of $\cdot O_2^-$, further confirming the evolution of $^1O_2$ from $\cdot O_2^-$. The slightly decreased reduction rate in the presence of TBA suggests the formation of quinone derivatives should be partly caused by $\cdot OH$. It was previously reported that $\cdot OH$, together with O_2, could also oxidize phenol to HQ (Equation 6).[54] However, the presence of $\cdot OH$ capturer TBA in the mixed reaction system does not cause the disappearance of the PBQ signal in the HPLC chromatogram (Figure 5a), demonstrating HQ should be mainly oxidized from phenol by $^1O_2$. The accelerated Cr(VI) reduction in the presence of $Na_2C_2O_4$ should result from the formation of $\cdot CO_2^-$ radicals with reducibility to Cr(VI).[55]

$$^1O_2 + \text{Phenol} \rightarrow \text{HQ} \quad (2)$$

$$\text{Cr(VI)} + \text{HQ} \leftrightarrows \text{Cr(III)} + \text{SQ} \quad (3)$$

$$\text{Cr(VI)} + \text{SQ} \leftrightarrows \text{Cr(III)} + \text{PBQ} \quad (4)$$

$$\text{PBQ} + \cdot O_2^- \rightarrow \text{SQ} \quad (5)$$

$$\cdot OH + O_2 + \text{Phenol} \rightarrow \text{HQ} + HO_2 \cdot \quad (6)$$

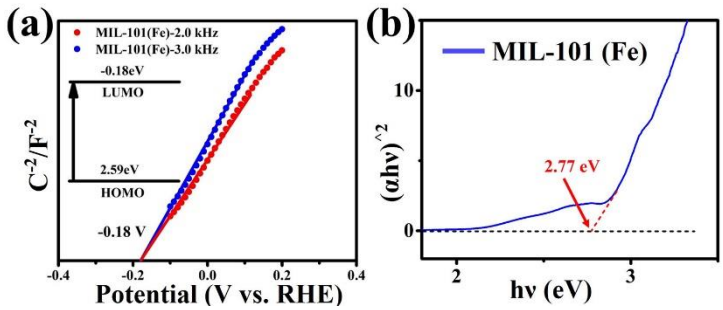

Figure 6. (a) Mott-Schottky plots for MIL-101(Fe) in a 0.1 M Na_2SO_4 aqueous solution; (b) bandgap determination for (MIL-101(Fe).

To understand the relation between the carrier transfer in the Ag/AgCl/MIL-101(Fe) composite and the evolution of active oxygen species, the electrochemical characteristics were further studied through Mott-Schottky measurements performed at the frequencies of 2000 and 3000 Hz. The intersection point is independent of the

frequency and the flat band position determined from the intersection is -0.18 V (Figure 6a), which is approximately used as the conduction band minimum (CBM). The bandgap of MIL-101(Fe) is 2.77 V according to the Tauc plot (Figure 6b), and the calculated valence band maximum (VBM) is 2.59 V.[56-58] The CBM and VBM levels of AgCl are -0.06 and 3.19 V according to the previous reports,[59] indicating AgCl can not be excited by the visible light. According to the improved Ag content during the first-run photocatalytic process, it is assumed the visible-light-excited MIL-101(Fe) may first transfer electrons to AgCl in the initial stage of photocatalysis, quickly improving the Ag content and enhancing the SPR effect of the composite. The electrons excited from plasmonic Ag NPs then transfer to the conduction band of AgCl and form $\cdot O_2^-$. Meanwhile, the electrons from MIL-101(Fe) are supposed to transfer to Ag and compensate the hole, stabilizing the electronic state of plasmonic Ag. The hole that remained in MIL-101(Fe) is supposed to result in a higher Fe(III) after the photocatalytic reaction. However, the contents of Fe(II) and Fe(III) sample keeps stable in the subsequent cyclic reactions. It is thus assumed that the in situ formed Fe(III) should further react with $\cdot O_2^-$, simultaneously forming $^1O_2$ and reducing Fe(III) to Fe(II) (Eq. 7, 8).

$$\mathrm{Fe(II)} + \mathrm{h^+} \rightarrow \mathrm{Fe(III)} \quad (7)$$

$$\mathrm{Fe(III)} + \cdot O_2^- \longrightarrow \mathrm{Fe(II)} + {}^1O_2 \quad (8)$$

Furthermore, the relation between $^1O_2$ and Cr(VI) reduction was analyzed based on the above assumption. First, according to the LC-MS analysis, both quinone derivatives (HQ, PBQ, SQ) and ring-opening products (fumaric acid, maleic acid, oxalic acid, etc.) can be detected (Table S2, Figure S12). The possible step-by-step degradation process of phenol is shown in Figure S13. Quinone derivatives are commonly observed in the presence of active oxygen species, including $\cdot OH$ and $^1O_2$. Since $\cdot OH$ radical has a higher oxidation potential, most of the quinone derivatives should be attacked by $\cdot OH$ and more deeply oxidized to ring-opening products in the initial phase. The Cr(VI) reduction was dramatically promoted until over 70% of phenol was oxidized. Therefore,

it is assumed that with the consumption of holes to form OH in the initial stage, O_2^- should be gradually accumulated and evolved into $^1O_2$. More quinone derivatives are then produced, which promote Cr(VI) reduction in the lagged stage.

The reducibility of quinone derivatives can be enhanced in the strong acidic system.[6, 7] To more explicitly demonstrate the effect of quinone derivatives on Cr(VI) reduction, the influence of pH variation on the Cr(VI) reduction was further explored during the photocatalysis. Sample 1% Ag/AgCl/MIL-101(Fe) used here has an isoelectric point of 4.2 (Figure S14). The original pH value of the phenol-Cr(VI) mixture is 3.8 and tuned to 6.0 to exclude the electrostatic adsorption. The pH decreased to ca. 4.6 in the first 30 min and finally reached 4.2 (Figure S15a), which verifies the photo-induced electron is not the main active species for Cr(VI) reduction. Photo-induced electrons should cause the slow Cr(VI) reduction in the initial stage through the random collision between photocatalyst and Cr(VI). The effect of decreased pH on the reduction ability of quinone derivatives was explored over the HQ-Cr(VI) mixture. The original pH value of HQ-Cr(VI) mixture was ca. 4.2 and tuned to 6.0 (Figure S15b). The Cr(VI) reduction efficiency was not obviously influenced by the initial pH value of the mixture, demonstrating the decreased pH in the phenol-Cr(VI) mixture under continuous irradiation is not responsible for the enhanced Cr(VI) reduction.

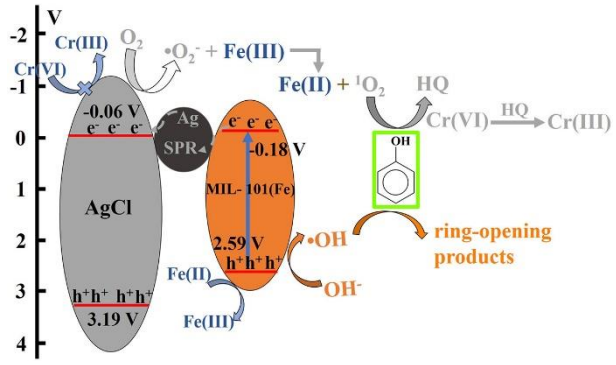

Scheme 2. Proposed photocatalytic mechanism.

3.4. Photocatalytic mechanism. Based on the above results, we proposed the photocatalytic mechanism of Ag/AgCl/MIL-101(Fe) for the combined treatment of phenol and Cr(VI) (Scheme 2). Under the irradiation of visible light, both Ag and MIL-

101(Fe) can be excited. The hot electrons can be produced from Ag benefitting from the SPR effect and charged to AgCl, which lead to the formation of $\cdot O_2^-$. The photo-induced electrons can not efficiently reduce anion Cr(VI) due to the poor surface adsorption. Meanwhile, the electrons excited from MIL-101(Fe) can be charged to Ag and keeps it active under the visible light irradiation. The holes remained in MIL-101(Fe) oxidize Fe(II) to Fe(III) and surface hydroxyls to $\cdot OH$. Fe(III) species further induces the formation of $^1O_2$ from $\cdot O_2^-$. Both $\cdot OH$ and $^1O_2$ oxidize phenol to quinone derivatives, and aggressive $\cdot OH$ radicals further cause the ring-opening and mineralization of quinone derivatives, which are more consumed in the initial phase. Quinone derivatives oxidize from $^1O_2$ are then accumulated and promote the Cr(VI) reduction in the lagged phase.

4. CONCLUSION.

In summary, ternary heterojunction Ag/AgCl/MIL-101(Fe) was formed by simply mixing Ag with MIL-101(Fe). This composite showed a cooperative effect for phenol degradation and Cr(VI) reduction. ·OH is responsible for the phenol degradation and the quinone derived from the reaction between phenol and $^1O_2$ significantly promotes Cr(VI) reduction. This study discriminates the effect of quinone derivatives on the Cr(VI) reduction from that of photo-induced electrons during the photocatalytic treatment of phenol-Cr(VI) mixture. It provides a joint treatment strategy for the phenol-Cr(VI) mixture that is not limited by the prerequisite for surface adsorption of metal ions on the catalyst surface. Moreover, the application of MOFs in water pollutant treatment has been commonly restricted by the poor carrier separation efficiency and instability. Here, the cooperation between SPR-Ag, conjugated AgCl and MOF-101(Fe) provides an efficient way for achieving excellent carrier separation and improving the photo-stability.

ASSOCIATED CONTENT

Supporting Information.

The Supporting Information is available free of charge at DOI: XXXXX.

SEM, HRTEM, The comparison of kinetic constants, UV-vis DRS, Photocurrent and EIS spectral analyses, N_2 adsorption-desorption isotherm and corresponding pore size, single Cr(VI) reduction and phenol degradation, XPS spectral analysis, effect of HQ and PBQ addition on the Cr(VI) reduction, possible intermediates in phenol degradation, MS spectra, degradation process of phenol, the isoelectric point, the change of pH value, apparent quantum efficiency of Cr(VI) (PDF)

AUTHOR INFORMATION

Corresponding Author

Tel.: +86 21 64252062; Fax: +86 21 64252062. E-mail: wlz@ecust.edu.cn;

Author Contributions

Jianqiu Gong and Weiwei Zhang contributed equally to this work. The manuscript was written with contributions from all authors. All authors have approved the final version of the manuscript.

Notes

The authors declare no competing financial interest.

ACKNOWLEDGMENT.

This work was supported by the Science and Technology Commission of Shanghai Municipality (18520710200, 20DZ2250400), the National Natural Science Foundation of China (21972040, 21673073), Shanghai Pujiang Program (18PJD012), Project supported by Shanghai Municipal Science and Technology Major Project (No.2018SHZDZX03) and the Program of Introducing Talents of Discipline to Universities (No. B20031, B16017).

REFERENCES

(1) Diao, Z. H.; Xu, X. R.; Jiang, D.; Kong, L. J.; Sun, Y. X.; Hu, Y. X.; Hao, Q. W.; Chen, H. Bentonite-supported nanoscale zero-valent iron/persulfate system for the simultaneous removal of Cr(VI) and phenol from aqueous solutions. *Chem. Eng. J.* **2016**, 302, 213-222.
(2) Gładysz-Płaska, A.; Majdan, M.; Pikus, S.; Sternik, D. Simultaneous adsorption of chromium(VI) and phenol on natural red clay modified by HDTMA. *Chem. Eng. J.* **2012**, 179, 140-150.
(3) Lu, D.; Chai, W.; Yang, M.; Fang, P.; Wu, W.; Zhao, B.; Xiong, R.; Wang, H. Visible light induced photocatalytic removal of Cr(VI) over TiO_2-based nanosheets loaded with surface-enriched CoO_x nanoparticles and its synergism with phenol oxidation. *Appl. Catal. B-Environ.* **2016**, 190, 44-65.
(4) Aksu, Z.; Gönen, F. Binary biosorption of phenol and chromium(VI) onto immobilized activated sludge in a packed bed: Prediction of kinetic parameters and breakthrough curves. *Sep. Purif. Technol.* **2006**, 49, 205-216.
(5) Chirwa, E. N.; Wang, Y. T. Simultaneous chromium(VI) reduction and phenol degradation in an anaerobic consortium of bacteria. *Water Res.* **2000**, 34, 2376-2384.
(6) Elovitz, M. S.; Fish, W. Redox Interactions of Cr(VI) and Substituted Phenols: Kinetic Investigation. *Environ. Sci. Technol.* **1994**, 28, 2161-2169.
(7) Elovitz, M. S.; Fish, W. Redox interactions of Cr (VI) and substituted phenols: products and mechanism. *Environ. Sci. Technol.* **1995**, 29, 1933-1943.
(8) Dozzi, M. V.; Saccomanni, A.; Selli, E. Cr(VI) photocatalytic reduction: Effects of simultaneous organics oxidation and of gold nanoparticles photodeposition on TiO_2. *J. Hazard. Mater.* **2012**, 211, 188-195.
(9) Lee, S. M.; Lee, T. W.; Choi, B. J.; Yang, J. K. Treatment of Cr(VI) and Phenol by Illuminated TiO_2. *J. Environ. Sci. Heal. A* **2003**, 38, 2219-2228.
(10) Wang, L.; Wang, N.; Zhu, L.; Yu, H.; Tang, H. Photocatalytic reduction of Cr(VI) over different TiO_2 photocatalysts and the effects of dissolved organic species. *J. Hazard. Mater.* **2008**, 152, 93-99.
(11) Liu, F.; Yu, J.; Tu, G.; Qu, L.; Xiao, J.; Liu, Y.; Wang, L.; Lei, J.; Zhang, J. Carbon nitride coupled Ti-SBA15 catalyst for visible-light-driven photocatalytic reduction of Cr (VI) and the synergistic oxidation of phenol. *Appl. Catal. B-Environ.* **2017**, 201, 1-11.
(12) Liang, H.; Li, T.; Zhang, J.; Zhou, D.; Hu, C.; An, X.; Liu, R.; Liu, H. 3-D hierarchical Ag/ZnO@CF for synergistically removing phenol and Cr(VI): Heterogeneous vs. homogeneous photocatalysis. *J. Colloid Interf. Sci.* **2020**, 558, 85-94.
(13) Fu, H.; Lu, G.; Li, S. Adsorption and photo-induced reduction of Cr (VI) ion in Cr (VI)-4CP (4-chlorophenol) aqueous system in the presence of TiO_2 as photocatalyst. *J. Photoch. Photobio. A* **1998**, 114, 81-88.
(14) Sun, K.; Jia, F.; Yang, B.; Lin, C.; Li, X.; Song, S. Synergistic effect in the reduction of Cr(VI) with Ag-MoS_2 as photocatalyst. *Appl. Mater Today* **2020**, 18, 100453.

(15) Borthakur, P.; Boruah, P. K.; Das, M. R.; Artemkina, S. B.; Poltarak, P. A.; Fedorov, V. E. Metal free MoS_2 2D sheets as a peroxidase enzyme and visible-light-induced photocatalyst towards detection and reduction of Cr(VI) ions. *New J. Chem.* **2018**, 42, 16919-16929.
(16) Hu, C.; Huang, Y. C.; Chang, A. L.; Nomura, M. Amine functionalized ZIF-8 as a visible-light-driven photocatalyst for Cr(VI) reduction. *J. Colloid Interf. Sci.* **2019**, 553, 372-381.
(17) Sahoo, D. P.; Patnaik, S.; Rath, D.; Parida, K. M. Synergistic effects of plasmon induced $Ag@Ag_3VO_4$/ZnCr LDH ternary heterostructures towards visible light responsive O_2 evolution and phenol oxidation reactions. *Inorg. Chem. Front.* **2018**, 5, 879.
(18) Sahoo, D. P.; Patnaik, S.; Parida, K. M. Construction of a Z-Scheme Dictated WO_3-X/Ag/ZnCr LDH Synergistically Visible Light-Induced Photocatalyst towards Tetracycline Degradation and H_2 Evolution. *ACS Omega* **2019**, 4, 14724-14741.
(19) Subudhi, S.; Swain, G.; Tripathy, S. P.; Parida, K. M. UiO-66-NH_2 Metal-Organic Frameworks with Embedded MoS_2 Nanoflakes for Visible-Light-Mediated H_2 and O_2 Evolution. *Inorg. Chem.* **2020**, 59, 9824-9837.
(20) Subudhi, S.; Mansingh, S.; Swain, G.; Behera, A.; Rath, D.; Parida, K. M. HPW-Anchored UiO-66 Metal-Organic Framework: A Promising Photocatalyst Effective toward Tetracycline Hydrochloride Degradation and H_2 Evolution via Z-Scheme Charge Dynamics. *Inorg. Chem.* **2019**, 58, 4921-4934.
(21) Subudhi, S.; Mansingh, S.; Tripathy, S. P.; Mohanty, A.; Mohapatra, P.; Rathd, D.; Parida, K. M. The fabrication of Au/Pd plasmonic alloys on UiO66-NH_2: an efficient visible light-induced photocatalyst towards the Suzuki Miyaura coupling reaction under ambient conditions. *Catal. Sci. Technol.* **2019**, 9, 6585.
(22) Patnaik, S.; Swain, G.; Parida K. M. Highly efficient charge transfer through a double Z-scheme mechanism by a Cu-promoted MoO_3/g-C_3N_4 hybrid nanocomposite with superior electrochemical and photocatalytic performance. *Nanoscale* **2018**, 10, 5950.
(23) Gao, Z.; Yang, H.; Fu, X.; Jin, Q.; Wu, Q.; Kang, L.; Wu, J. Efficient photoreduction of Cr(VI) on TiO_2/functionalized activated carbon (TiO_2/AC-AEMP): improved adsorption of Cr(VI) and induced transfer of electrons. *Environ. Sci. Pollut. R.* **2020**, 27, 17446-17457.
(24) Li, X.; Chen, D.; Li, N.; Xu, Q.; Li, H.; He, J.; Lu, J. Efficient reduction of Cr(VI) by a BMO/Bi_2S_3 heterojunction via synergistic adsorption and photocatalysis under visible light. *J. Hazard. Mater.* **2020**, 400, 123243.
(25) Gao, Y.; Chen, C.; Tan, X.; Xu, H.; Zhu, K. Polyaniline-modified 3D-flower-like molybdenum disulfide composite for efficient adsorption/photocatalytic reduction of Cr(VI). *J. Colloid Interf. Sci.* **2016**, 476, 62-70.
(26) Yang, Y.; Li, J.; Yan, T.; Zhu, R.; Yan, L.; Pei, Z. Adsorption and photocatalytic reduction of aqueous Cr(VI) by Fe_3O_4-ZnAl-layered double hydroxide/TiO_2 composites. *J. Colloid Interf. Sci.* **2020**, 562, 493-501.

(27) He, X.; Chi, H.; He, M.; Zhang, B.; Zhang, J.; Wang, D.; Ma, J. Efficient removal of halogenated phenols by vacuum-UV system through combined photolysis and OH oxidation: Efficiency, mechanism and economic analysis. *J. Hazard. Mater.* **2021**, 403, 123286.
(28) Xu, C.; Wang, L. Atmospheric Oxidation Mechanism of Phenol Initiated by OH Radical. *J. Phys. Chem. A* **2013**, 117, 2358-2364.
(29) Yazdanbakhsh, A.; Aliyari, A.; Sheikhmohammadi, A.; Aghayani, E. Application of the enhanced sono-photo-Fenton-like process in the presence of persulfate for the simultaneous removal of chromium and phenol from the aqueous solution. *J. Water Process Eng.* **2020**, 34, 101080.
(30) Xu, T.; Lu, W.; Wu, X. F.; Chen, W.; Solar-driven conversion of arylboronic acids to phenols using metal-free heterogeneous photocatalysts. *J. Catal.* **2019**, 378, 63-67.
(31) Piwowar, K.; Blacha-Grzechnik, A.; Bernas, P.; Zak, J. Phenol degradation in heterogeneous system generating singlet oxygen employing light activated electropolymerized phenothiazines. *Appl. Surf. Sci.* **2015**, 359, 426-431.
(32) Zhou, Y.; Jiang, J.; Gao, Y.; Pang, S. Y.; Yang, Y.; Ma, J.; Gu, J.; Li, J.; Wang, Z.; Wang, L. H.; Yuan, L. P.; Yang, Y. Activation of peroxymonosulfate by phenols: Important role of quinone intermediates and involvement of singlet oxygen. *Water Res.* **2017**, 125, 209-218.
(33) Tian, X.; Gao, P.; Nie, Y.; Yang, C.; Zhou, Z.; Li, Y.; Wang, Y. A novel singlet oxygen involved peroxymonosulfate activation mechanism for degradation of ofloxacin and phenol in water. *Chem. Commun.* **2017**, 53, 6589-6592.
(34) Feng, J.; Li, S.; Sheng, Y.; Xiong, Y.; Lan, S.; Tian, S.; Kong, L.; Fan, C. Remarkable improvement of cycling Fenton process for catalytic degradation of phenol: Tuning of triggering effect. *Appl. Catal. A-Gen.* **2017**, 542, 21-27.
(35) Lv, K.; Guo, X.; Wu, X.; Li, Q.; Ho, W.; Li, M.; Ye, H.; Du, D. Photocatalytic selective oxidation of phenol to produce dihydroxybenzenes in a TiO_2/UV system: Hydroxyl radical versus hole. *Appl. Catal. B-Environ.* **2016**, 199, 405-411.
(36) Minero, C.; Mariella, G.; Maurino, V.; Pelizzetti, E. Photocatalytic transformation of organic compounds in the presence of inorganic anions. 1. Hydroxyl-mediated and direct electron-transfer reactions of phenol on a titanium dioxide -fluoride system. *Langmuir* **2000**, 16, 2632-2641.
(37) Chen, C.; Zhao, W.; Lei, P.; Zhao, J.; Serpone, N. Photosensitized Degradation of Dyes in Polyoxometalate Solutions Versus TiO_2 Dispersions under Visible-Light Irradiation: Mechanistic Implications. *Chem-Eur J.* **2004**, 10, 1956-1965.
(38) Yi, Q.; Ji, J.; Shen, B.; Dong, C.; Liu, J.; Zhang, J.; Xing, M. Singlet Oxygen Triggered by Superoxide Radicals in a Molybdenum Cocatalytic Fenton Reaction with Enhanced Redox Activity in the Environment. *Environ. Sci. Technol.* **2019**, 53, 9725-9733.
(39) Jedsukontorn, T.; Meeyoo, V.; Saito, N.; Hunsom, M. Effect of electron acceptors H_2O_2 and O_2 on the generated reactive oxygen species $^1O_2$ and OH in TiO_2-catalyzed photocatalytic oxidation of glycerol. *Chinese J. Catal.* **2016**, 37, 1975-1981.

(40) Alvaro, M.; Carbonell, E.; Ferrer, B.; Llabrés i Xamena, F. X.; Garcia, H. Semiconductor Behavior of a Metal-Organic Framework (MOF). *Chem-Eur. J.* **2007**, 13, 5106-5112.
(41) Xamena, F. X. L. I.; Corma, A.; Garcia, H. Applications for Metal-Organic Frameworks (MOFs) as Quantum Dot Semiconductors. *J. Phys. Chem. C* **2007**, 111, 80-85.
(42) Pu, S.; Xu, L.; Sun, L.; Du, H. Tuning the optical properties of the zirconium-UiO-66 metal-organic framework for photocatalytic degradation of methyl orange. *Inorg. Chem. Commun.* **2015**, 52, 50-52.
(43) Jing, H. P.; Wang, C. C.; Zhang, Y. W.; Wang, P.; Li, R. Photocatalytic degradation of methylene blue in ZIF-8. *RSC Adv.* **2014**, 4, 54454-54462.
(44) Sha, Z.; Chan, H. S. O.; Wu, J. Ag_2CO_3/UiO-66(Zr) composite with enhanced visible-light promoted photocatalytic activity for dye degradation. *J. Hazard. Mater.* **2015**, 299, 132-140.
(45) Du, D. Y.; Qin, J. S.; Li, S. L.; Su, Z. M.; Lan, Y. Q. J. C. S. R. Recent advances in porous polyoxometalate-based metal-organic framework materials. *Chem. Soc. Rev.* **2014**, 43, 4615-4632.
(46) Xuan, W.; Zhu, C.; Liu, Y.; Cui, Y. J. C. S. R. Mesoporous metal-organic framework materials. *Chem. Soc. Rev.* **2012**, 41, 1677-1695.
(47) Salunkhe, R. R.; Kaneti, Y. V.; Yamauchi, Y. J. A. N. Metal-organic framework-derived nanoporous metal oxides toward supercapacitor applications: progress and prospects. *ACS Nano.* **2017**, 11, 5293-5308.
(48) Toyao, T.; Saito, M.; Dohshi, S.; Mochizuki, K.; Iwata, M.; Higashimura, H.; Horiuchi, Y.; Matsuoka, M. J. C. C. Development of a Ru complex-incorporated MOF photocatalyst for hydrogen production under visible-light irradiation. *Chem. Commun.* **2014**, 50, 6779-6781.
(49) Zhao, M.; Yuan, K.; Wang, Y.; Li, G.; Guo, J.; Gu, L.; Hu, W.; Zhao, H.; Tang, Z. Metal-organic frameworks as selectivity regulators for hydrogenation reactions. *Nature* **2016**, 539, 76-80.
(50) Weckhuysen, B. M.; Wachs, I. E.; Schoonheydt, R. A. Surface Chemistry and Spectroscopy of Chromium in Inorganic Oxides. *Chem. Rev.* **1996**, 96, 3327-3350.
(51) Salunkhe, R. R.; Kaneti, Y. V.; Yamauchi, Y. Metal-organic framework-derived nanoporous metal oxides toward supercapacitor applications: progress and prospects. *ACS Nano.* **2017**, 11, 5293-5308.
(52) Bordiga, S.; Lamberti, C.; Ricchiardi, G.; Regli, L.; Bonino, F.; Damin, A.; Lillerud, K.-P.; Bjorgen, M.; Zecchina, A. Electronic and vibrational properties of a MOF-5 metal-organic framework: ZnO quantum dot behaviour. *Chem. Commun.* **2004**, 20, 2300-2301.

(53) Han, S. K.; Bilski, P.; Karriker, B.; Sik, R. H.; Chignell, C. F. Oxidation of flame retardant tetrabromobisphenol A by singlet oxygen. *Environ. Sci. Technol.* **2008**, 42, 166-172.

(54) Chen, R.; Pignatello, J. J. Role of quinone intermediates as electron shuttles in Fenton and photoassisted Fenton oxidations of aromatic compounds. *Environ. Sci. Technol.* **1997**, 31, 2399-2406.
(55) Ren, H.; Hou, Z.; Han, X.; Zhou, R. Highly reductive radical CO_2-deriving from a system with SO_4^- and formate anion: Implication for reduction of Cr(VI) from wastewater. *Chem. Eng. J.* **2017**, 309, 638-645.
(56) Lu Z.; Zhou G.; Song M.; Liu X.; Tang H.; Dong H.; Huo P.; Yan F.; Du P.; Xing G. Development of magnetic imprinted PEDOT/CdS heterojunction photocatalytic nanoreactors: 3-Dimensional specific recognition for selectively photocatalyzing danofloxacin mesylate. *Appl. Catal. B-Environ.* **2020**, 268, 118433
(57) Lu Z.; Zhou G.; Song M.; Wang D.; Huo P.; Fan W.; Dong H.; Tang H.; F. Yan; Xing G. Magnetic functional heterojunction reactors with 3D specific recognition for selective photocatalysis and synergistic photodegradation in binary antibiotic solutions. *J. Mater. Chem. A* **2019**, 7, 13986-14000
(58) He F.; Lua Z.; Song M.; Liu X.; Tang H.; Huo P.; Fan W.; Dong H.; Wu X.; Han S. Selective reduction of Cu^{2+} with simultaneous degradation of tetracycline by the dual channels ion imprinted POPD-$CoFe_2O_4$ heterojunction photocatalyst. *Chem. Eng. J.* **2019**, 360, 750-761
(59) Li, X.; Wu, D.; Luo, Q.; Yin, R.; An, J.; Liu, S.; Wang, D. Fabrication of CPAN/Ag/AgCl composites and their efficient visible-light photocatalytic activity. *J. Alloy Compd.* **2017**, 702, 585-593.

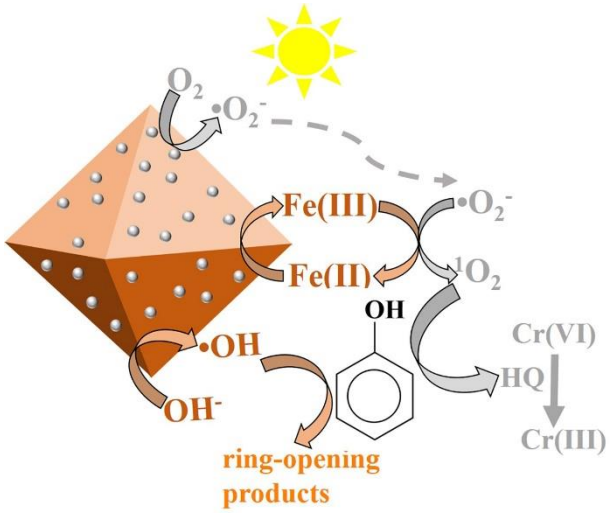

The TOC graph